Coupling of Navier-Stokes Equations and Their Hydrostatic Versions and Simulation of Riverbend Flow

Wenbin Dong, Hansong Tang, and Yingjie Liu

1 Introduction

It has become necessary to develop modeling capabilities to simulate multiscale, multiphysics ocean flows directly. An example of such flows is the 2010 Gulf of Mexico oil spill, in which the spill started as a high-speed plume at the seabed and then it evolved into drifting oil patches on the ocean surface [1]. Since the plume and the patches are phenomena distinct in physics at temporal and spatial scales and better described by different sets of partial differential equations (PDEs), they are referred to as multiscale and multiphysics flows [2, 3].

Coupling the Navier-Stokes (NS) equations, which describe complex small-scale local flows, and hydrostatic versions of the Navier-Stokes (HNS) equations, which depict the large-scale background ocean flows, is a natural approach to realize simulations of multiscale and multiphysics ocean flows. Example topics of efforts on such coupling include optimized interface conditions for convergence speedup of Schwarz iteration between the NS and HNS equations [4], appropriate interface conditions [5], simulation of multiscale, multiphysics ocean flows [6, 7, 2, 8, 9], etc. Due to the complexity of the coupling, these earlier efforts are mostly simple and crude in methods (e.g., one-way coupling), and they are sporadic in both theoretical analysis and desired computation implementation (particularly two-way coupling). Actually, problems such as non-physical solutions have been reported in simulations

Wenbin Dong

Civil Engineering Department, City College, City University of New York, NY 10031, USA. e-mail: `wdong000@citymail.cuny.edu`

Hansong Tang*, corresponding author

Civil Engineering Department, City College, City University of New York, NY 10031, USA. e-mail: `htang@ccny.cuny.edu`

Yingjie Liu

School of Mathematics, Georgia Institute of Technology, Atlanta, GA 30332, USA. e-mail: `yingjie@math.gatech.edu`

based on such coupling [10]. A more detailed review can be found in [8, 9]. It is fair to say that we are still at an exploration stage of such coupling.

This work presents a discussion on the coupling of the NS and HNS equations to capture physical phenomena correctly. A numerical example is provided to illustrate the necessity for coupling the NS and HNS equations and the influence of different transmission conditions.

2 Governing Equations

A flow domain, Ω_0, is divided into a near field assigned with the NS equations, Ω_{NS}, and a far field applied with the NHS equations, Ω_{HNS}, see Fig. 1. The near field wraps a small-scale, complex, local flow, and the far field covers its large-scale background flow. For a near field, the governing equations consist of the continuity equation and the NS equations [8, 11]:
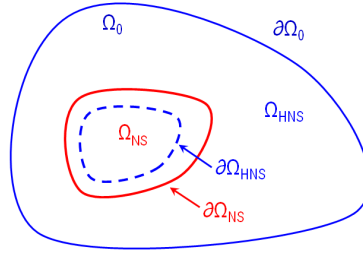

Fig. 1: Division of flow domain, Ω_0 ($= \Omega_{NS} \cup \Omega_{HNS}$). $\partial\Omega_0$ is its boundary, and $\partial\Omega_{NS}$ and $\partial\Omega_{HNS}$ are the interfaces for the NS and HNS equations, respectively.

$$
\begin{aligned}
&\nabla \cdot \mathbf{u} = 0 \\
&\mathbf{u}_t + \nabla \cdot \mathbf{uu} = \nabla \cdot ((\nu + \nu_t) \, \nabla \, \mathbf{u}) - \nabla p_d / \rho - g \, \nabla_H \, \eta
\end{aligned}
\tag{1}
$$

Here, $\mathbf{u} = (u, v, w)$, the velocity vector, with u and v as its components in x and y direction, respectively, on the horizontal plane, and w as its component in z direction, or, the vertical direction. η is the water surface elevaiton, and $p_d = p - \rho g(\eta - z)$, with p being pressure. ν is the viscosity, ν_t the turbulence viscosity, ρ the density, and g the gravity. ∇_H is the gradient in the horizontal plane. When $\rho = const$, p_d becomes the dynamic pressure, and it is introduced to facilitate the coupling of the NS to the HNS equations [8].

In a far field, the governing equations are the continuity equation and the HNS equations (the latter is simplified from the NS equations according to the hydrostatic assumption, i.e., $p = \rho g(\eta - z)$), and they read as

$$
\begin{aligned}
&\nabla \cdot \mathbf{u} = 0 \\
&\mathbf{v}_t + \nabla \cdot \mathbf{uv} = \nabla \cdot ((\nu + \nu_t) \, \nabla \, \mathbf{v}) - g \, \nabla_H \, \eta
\end{aligned}
\tag{2}
$$

where $\mathbf{v} = (u, v)$, the velocity vector in the horizontal plane.

As a practical approach, the following interface conditions are adopted in computation:

$$
\begin{aligned}
\mathbf{u}|_{NS} = \mathbf{u}|_{HNS}, \ \partial p_d/\partial n = 0, \quad &\text{on } \partial\Omega_{NS} \\
\mathbf{u}|_{HNS} = \mathbf{u}|_{NS}, \quad &\text{on } \partial\Omega_{HNS}
\end{aligned} \tag{3}
$$

which requires the continuity of $\mathbf{u}$ across an interface. Another approach is

$$
\begin{aligned}
\left(\mathbf{u}_n\mathbf{v} + p_{d_n}/\rho - (\nu + \nu_t)\partial\mathbf{v}/\partial n\right)|_{NS} & \\
= (\mathbf{u}_n\mathbf{v} - (\nu + \nu_t)\partial\mathbf{v}/\partial n)|_{HNS}, \quad &\text{on } \partial\Omega_{NS} \\
\mathbf{u}_\tau|_{NS} = \mathbf{u}_\tau|_{HNS}, \ \partial p_d/\partial n = 0, \quad &\text{on } \partial\Omega_{NS} \\
\mathbf{u}|_{HNS} = \mathbf{u}|_{NS}, \quad &\text{on } \partial\Omega_{HNS}
\end{aligned} \tag{4}
$$

here subscript τ indicates the tangential direction. (4) is same to (3) except that, on an interface of the NS equations and in its normal direction, the continuity of velocity is replaced by continuity of momentum flux. Condition (4) is adopted/modified from previous investigations [4, 11].

3 Computational Methods

The NS equations (1) are computed using the Solver of Incompressible Flow on Overset Meshes (SIFOM) developed by us (e.g., [13, 12]). The solver discretizes the equations in curvilinear coordinates using a second-order accurate backward difference in time and central difference on non-staggered, composite structured grids [13]. The HNS equations are solved by utilizing the Finite Volume Method Coastal Ocean Model (FVCOM), which is an operational model in the ocean science community [14]. In this model, the HNS equations (2) are transformed and solved in the following form:

$$
\begin{aligned}
\eta_t + \nabla_H \cdot (\mathbf{v}D) + \omega_\sigma &= 0, \\
(\mathbf{v}D)_t + \nabla_H \cdot (\mathbf{v}\mathbf{v}D) + (\mathbf{v}\omega)_\sigma &= -gD\,\nabla_H\,\eta + \nabla_H \cdot (\kappa\mathbf{e}) \\
&\quad + (\lambda\mathbf{v}_\sigma)_\sigma/D + \mathbf{I},
\end{aligned} \tag{5}
$$

in which σ is a vertical coordinate, ω the vertical velocity in this coordinate, $\mathbf{e}$ the strain rate, subscript σ the derivative over σ, and $\mathbf{I}$ the other terms. κ and λ are coefficients. Actually, in FVCOM, equations (5) are solved together with another set of equations, which essentially result from integrating the NS equations in the vertical direction [14]. The model adopts the second-order accuarte Runge-Kutta method in time and a second-order accurate finite volume method on a triangular grid in the horizontal plane and a σ-grid in the vertical direction. The grids of SIFOM and FVCOM overlap arbitrarily with each other (i.e., Chimera grids), and their solutions are exchanged at interfaces between the two grids via interpolation [8].

Let the discretized NS and HNS equations be respectively expressed as

$$\mathbf{F}(\mathbf{f}) = \mathbf{0}, \quad \mathbf{H}(\mathbf{h}) = \mathbf{0} \tag{6}$$

in which $\mathbf{f} = (\mathbf{u}, p_d)$, and $\mathbf{h} = (\mathbf{v}, \omega, \eta)$, being the solution for the NS and HNS equations, respectively. Then, the computation of their coupling when marching from time level n to $n + 1$ is formulated as

$$\bar{\mathbf{f}}^0 = \mathbf{f}^n, \; \bar{\mathbf{h}}^0 = \mathbf{h}^n$$
$$Do\; 1\; m = 1, M$$

$$\begin{cases} \mathbf{F}(\bar{\mathbf{f}}^m) = \mathbf{0}, & \mathbf{x} \in \Omega_{NS} \\ \bar{\mathbf{f}}^m = \mathbf{p}(\mathbf{h}^{m-1}), & \mathbf{x} \in \partial\Omega_{NS} \end{cases} \quad \begin{cases} \mathbf{H}(\bar{\mathbf{h}}^m) = \mathbf{0}, & \mathbf{x} \in \Omega_{HNS} \\ \bar{\mathbf{h}}^m = \mathbf{q}(\mathbf{f}^{m-1}), & \mathbf{x} \in \partial\Omega_{HNS} \end{cases} \tag{7}$$

$$1\; End\; Do$$
$$\mathbf{f}^{n+1} = \bar{\mathbf{f}}^M, \; \bar{\mathbf{h}}^{n+1} = \bar{\mathbf{h}}^M$$

in which m is the Schwarz iteration index, and M is a prescribed integer. $\mathbf{p}$ and $\mathbf{q}$ are operators for solution exchange between the NS and HNS equations.

4 Numerical Simulation

Numerical experiments are made on a transient water flow in a riverbend, see Fig. 2. The water body is stationary initially, and it flows as velocity is imposed at its entrance, with the following initial and boundary conditions:

$$\mathbf{u} = 0, \; p = \gamma(\eta - z), \; t = 0$$
$$u = 0.25(1 - e^{-0.01t}), \; \text{at entrance}; \; \eta = 15, \; \text{at exit} \tag{8}$$

Here, length is in m, and time is in s, and velocity is in m/s.

The mesh for the HNS equations covers the whole channel, with 10,000 triangular cells in the horizontal plane and 20 layers in the vertical direction, and the grid for the NS equations occupies the bend section, with a grid of 111×13×13 in the streamwise, lateral, and vertical direction, respectively. The time step is set as $\Delta t = 0.01$, and $M = 1$ is used in (7).

The simulated instantaneous water surface elevation by the HNS equations and those by the coupled HNS and NS equations are depicted in Fig. 3. At $t = 60$, in the transient stage, the simulated elevations by both approaches are essentially identical. When $t = 1200$, at which the flow is about steady, the elevation obtained with the HNS/NS equations differs from that with the HNS equations in patterns. Additionally, the elevations computed by the coupled equations with interface conditions (3) and (4) are similar in main patterns, but they do have a little difference in magnitude.

Fig. 4 illustrates the velocity field at cross-section a-a in the curved section of the channel (Fig. 2). The figure shows that the HNS simulation presents a vortex covering the whole cross-section. Whereas the HNS/NS simulations lead to two counter-rotation vortices in the middle of the cross-section, plus one at the left
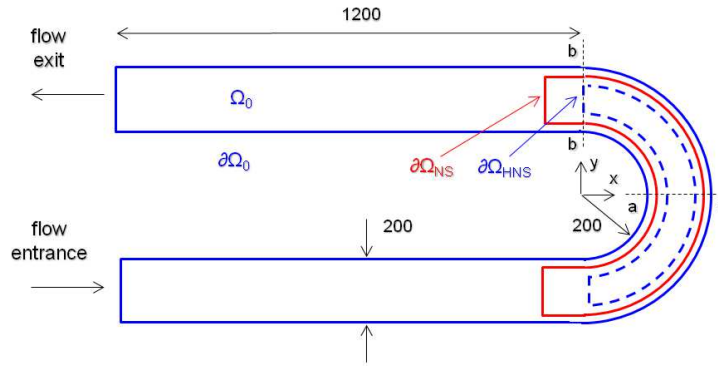
Fig. 2: Riverbend configuration and subdomains.

lower corner, one at the right lower corner, and one at the upper right corner. Such multiple vorticies have been reported in previous investigations based on the NS equations [15], and the difference indicates the necessity of the NS/HNS coupling. Additionally, it is seen that, with the coupled equations, although both interface conditions (3) and (4) lead to three vorticities on the cross-section, their positions have changed in some degree (Fig. 4). This indicates that interface conditions (3) and (4) could produce difference in solutions.

To further examine the difference, the vertically averaged velocities are plotted in Fig. 5. It is seen that the coupled HNS/NS equations provide solutions for both streamwise and lateral velocity that are distinct from those obtained with the HNS equations. Note the streamwise velocity is y-velocity and x-velocity at cross-section a-a and b-b, respectively. Moreover, the two interface conditions lead to similar streamwise velocities but distinct lateral velocities. To illustrate this with more details, we present a quantification of the difference in the solutions obtained with the two interface conditions in Table 1. The numbers in the table show that the difference in the lateral velocities is more pronounced, indicating that the two interface conditions lead to a big difference in the secondary flows in the bend's cross-section.

Table 1: Difference of the HNS/NS solutions obtained with different interface conditions. $\bar{u}$ and $\bar{v}$ are vertically integrated x- and y-velocity, respectively, and subscripts 3 and 4 depict interface condition (3) and (4), respectively.

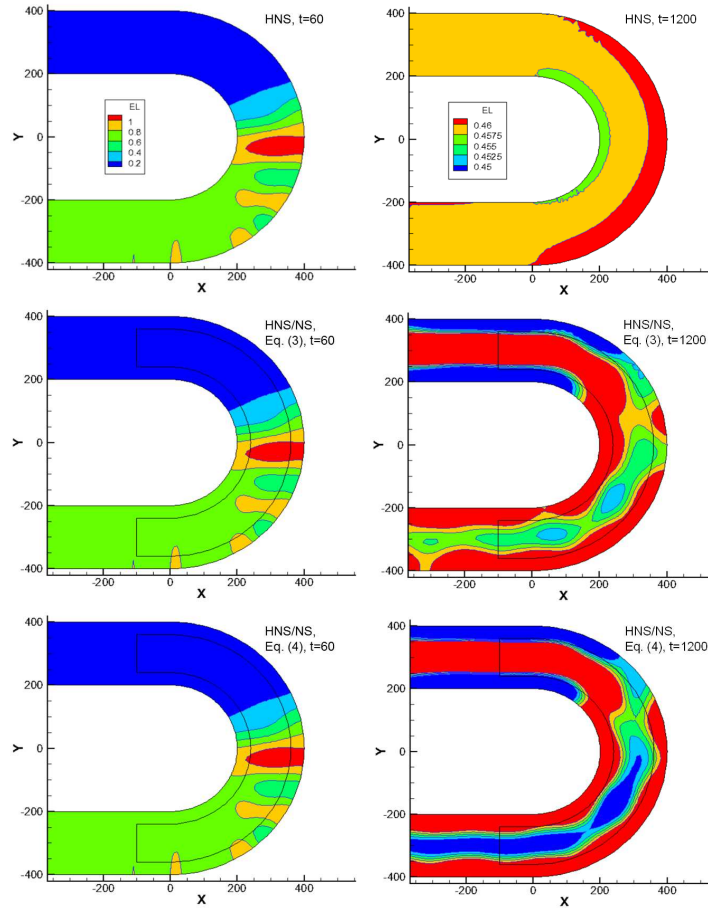| cross section	$\|\|\bar{u}_4 - \bar{u}_3\|\|_2/\|\bar{u}_3\|_{max}$	$\|\|\bar{v}_4 - \bar{v}_3\|\|_2/\|\bar{v}_3\|_{max}$
a-a	1.809	0.385
b-b	0.268	2.196

Fig. 3: Simulated instantaneous water surface elevation by the HNS equations and coupled NHS/NS equations with interface condition (3) and (4).

5 Concluding Remarks

We present a discussion on the coupling of the NHS and NS equations. The numerical experiment on a riverbend flow shows that the coupling can capture complex flow phenomena that the HNS equations cannot resolve. It also indicates that different interface conditions may lead to different solutions, especially those for the secondary flows in cross-sections of the bend.

Further investigation is necessary for the two transmission conditions in this paper. Particularly, examining their performance against benchmarks plus theoretical analysis is expected to be the next step, followed by domain decomposition techniques to achieve desired computational efficiency.
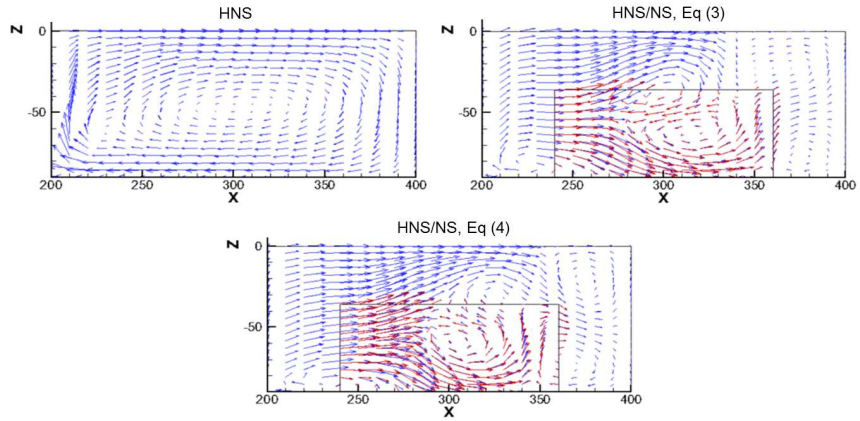
Fig. 4: Simulated cross-section flow field, at cross section a-a in Fig. 2, $t = 1200$.
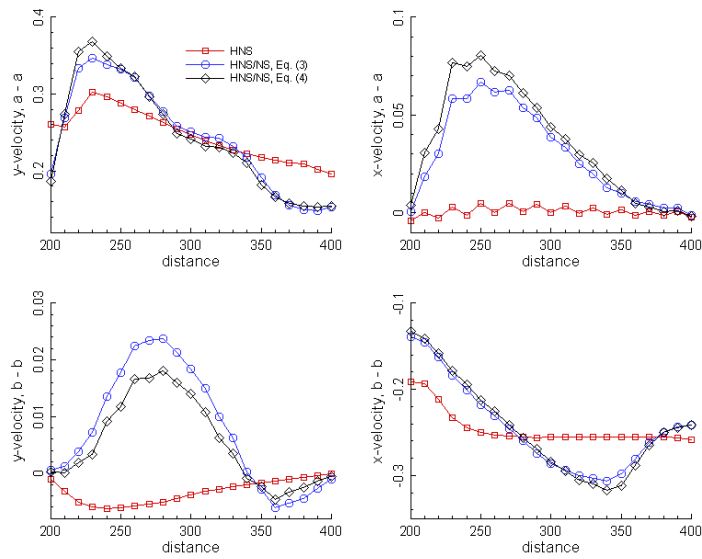

Fig. 5: Vertically averaged velocity at cross sections a-a and b-b in Fig. 2, $t = 1200$.

References

1. Camilli, R. and Reddy, C.M. and Yoerger, D.R. and Van Mooy and B.A.S. and Jakuba, M.V. and Kinsey, J.C. and McIntyre, C.P. and Sylva, S.P. and Maloney, J.V.: Tracking hydrocarbon plume transport and biodegradation at Deepwater Horizon. Science **330**, 208–211 (2010).
2. Tang, H.S. and Wu, X.G.: Multi-scale coastal flow simulation using coupled CFD and GFD models. In: Swayne, D.A., Yang, W., Voinov, A.A., Rizzoli, A., Filatova, T. (Eds.), Modelling for Environment's Sake, 5th Biennial Meeting. Ottawa, 2010.
3. Candy, A.S.: An implicit wetting and drying approach for non-hydrostatic baroclinic flows in high aspect ratio domains. Adv. Water Resour. **102**, 188–205 (2017).
4. Blayo, E. and Rousseau, A.: About interface conditions for coupling hydrostatic and nonhydro-static navier-stokes flows. Discrete and Continuous Dynamical Systems Series. **9**, 1565-1574 (2016).
5. Gallacher, P.C. and Hebert, D.A. and Schaferkotter, M. R.: Nesting a nonhydrostatic model in a hydrostatic model: The boundary interface, Ocean Modelling, **40**, 190-198 (2011).
6. Fujima, K. Masamura, K., and Goto. C.: Development of the 2D/3D hybrid model for tsunami numerical simulation, Coastal Eng J., **44**, 373-397 (2002).
7. Fringer, O.B. and McWilliams, J.C. and Street, R.L.: A new hybrid model for coastal simula-tions, Oceanography, **19**, 64-77 (2006).
8. Tang, H.S. and Qu, K. and Wu, X.G.: An overset grid method for integration of fully 3D fluid dynamics and geophysical fluid dynamics models to simulate multiphysics coastal ocean flows. J. Comput. Phys. **273**, 548 – 571 (2014).
9. Qu, K. and Tang, H. S. and Agrawal, A.: Integration of fully 3D fluid dynamics and geophysical fluid dynamics models for multiphysics coastal ocean flows: Simulation of local complex free-surface phenomena, Ocean Modelling, **135**, 14 –30 (2019).
10. Tang, H.S. and Qu, K. and Wu, X.G. and Zhang, Z.K.: Domain decomposition for a hybrid fully 3D fluid dynamics and geophysical fluid dynamics modeling system: A numerical experiment on a transient sill flow. In Dickopf, T. and Gander, M.J. and Halpern, L. and Krause, R. and Pavarino, L.F. (eds) Domain Decomposition Methods in Science and Engineering XXII. Lecture Notes in Computational Science and Engineering, **104**, Springer, 407-414 (2016).
11. Tang, H.S. and Liu, Y.J.: Coupling of Navier-Stokes equations and their hydrostatic versions for ocean flows: A discussion on algorithm and implementation. In Haynes, R., MacLachlan, S., Cai, X.-C., Halpern, L., Kim, H.H., Klawonn, A., Widlund, O. (eds) Domain Decomposition Methods in Science and Engineering XXV. Lecture Notes in Computational Science and Engineering, **138**, Springer, 326-333 (2020).
12. Ge, L. and Sotiropoulos, F.: 3D unsteady RANS modeling of complex hydraulic engineering flows. I: numerical model. J. Hydraul. Eng., **131**, 800–808 (2005).
13. Tang, H.S. and Jones, S.C. and Sotiropoulos, F.: An overset-grid method for 3D unsteady incompressible flows. J. Comput. Phys. **191**, 567-600 (2003).
14. Chen, C. and Liu, H. and Beardsley, R.C.: An unstructured, finite-volume, three-dimensional, primitive equation ocean model: application to coastal ocean and estuaries. J. Atm. & Oceanic Tech. **20**, 159-186(2003).
15. Li, B. and Zhang, X. and Tang, H.S. and Tsubaki, R.: Influence of deflection angles on flow behaviours in open channel bends. J. Mountain Science **15**, 2292-2306 (2018).